Nanoscale

Strong coupling of emitters to single plasmonic nanoparticles: Exciton-induced transparency and Rabi splitting

Journal:	*Nanoscale*
Manuscript ID	NR-FEA-06-2019-005044.R1
Article Type:	Feature Article
Date Submitted by the Author:	10-Jul-2019
Complete List of Authors:	Pelton, Matthew ; University of Maryland Baltimore County Storm, S. David; University of Maryland Baltimore County Leng, Haixu; University of Maryland Baltimore County College of Natural and Mathematical Sciences, Physics

FEATURE ARTICLE

Strong coupling of emitters to single plasmonic nanoparticles: Exciton-induced transparency and Rabi splitting

Received 00th January 20xx,
Accepted 00th January 20xx

DOI: 10.1039/x0xx00000x

Matthew Pelton,* S. David Storm and Haixu Leng

Strong coupling between plasmons in metal nanoparticles and single excitons in molecules or semiconductor nanomaterials has recently attracted considerable experimental effort for potential applications in quantum-mechanical and classical optical information processing and for fundamental studies of light-matter interaction. Here, we review the theory behind strong plasmon-exciton coupling and provide analytical expressions that can be used for fitting experimental data, particularly the commonly measured scattering spectra. We re-analyze published data using these expressions, providing a uniform method for evaluating and quantifying claims of strong coupling that avoids ambiguities in distinguishing between Rabi splitting and exciton-induced transparency (or Fano-like interference between plasmons and excitons).

Introduction and theory

There has recently been a surge of interest in strong coupling between plasmons in metal nanostructures and excitons in molecular or semiconductor materials. [1,2,3,4] Strong coupling, in this case, means that the coupling strength between excitons and plasmons exceeds damping rates in the coupled system, so that the excitons and plasmons form new, hybrid normal modes. The elementary excitations of the coupled system are then no longer excitons or plasmons, but combinations of the two. In particular, there has been a push to realize strong coupling at the level of single excitons coupled to single plasmonic nanostructures.

This represents a significant challenge. Not only is it a challenge to fabricate and optically probe single strongly-coupled nanostructures, but it is also not trivial to understand the often complex experimental spectra that result. In this Feature Article, we review published results for excitons coupled to single plasmonic nanostructures and determine which results correspond unambiguously to the strong-coupling regime. In order to explain how we examine the results, we first review the background and theory of plasmon-exciton coupling.

Weak coupling: the Purcell effect.

The motivation for observing strong plasmon-exciton coupling comes from the much longer-standing observation of enhanced luminescence from optical emitters coupled to plasmonic structures. The first such observations were made by Drexhage in the late 1960s, who measured increased in emission rates from layers of dye molecules at nanometer-scale distances from metal films.[5,6] The first widespread interest in metal-enhanced luminescence, however, came about a decade later, following the observation of surface-enhanced Raman scattering (SERS).[7,8] It was quickly understood that the massive signal enhancements in SERS were due to localization of optical fields through their coupling to plasmon resonances in roughened metal surfaces.[9] This same field localization was observed to enable the enhancement of other optical processes, including luminescence.[10,11] Although both increases and decreases in luminescence signal were observed in different experiments, the decay rate of the emitting species was uniformly observed to increase.[12,13]

Since these observations were first made by chemists, they were first described in their language of energy transfer.[12] In analogy to Förster resonant energy transfer (FRET), plasmon-enhanced emission can be understood as energy transfer from an excited excitonic state to plasmon resonances followed by radiative and non-radiative decay of the plasmons. Shortly afterwards, electrical engineers became interested in the phenomenon, and adopted the language of optical antennas.[14] This description, first developed in the context of near-field scanning optical microscopy (NSOM),[15,16] sees the plasmonic metal nanostructure as the optical-frequency analogue of a radio-wave or microwave antenna, broadcasting optical energy from an exciton to the far field.

In order to understand the connection between luminescence enhancement and strong coupling, perhaps the most useful description is in the physicist's language of cavity quantum electrodynamics (QED). At the same time as chemists were modifying the emission rate of molecules next to metal surfaces, physicists were modifying the emission rates of atoms in microwave[17] or optical[18] cavities. They explained the modification of emission rates as being due to a modification in the density of states, $\rho(\hbar\omega)$, available to the emitted photon: according to Fermi's golden rule,[19] the spontaneous emission rate is

$$\gamma_1 = \frac{2\pi}{\hbar}|V_{fi}|^2\rho(\hbar\omega)\,, \qquad (1)$$

where V_{fi} is the dipole transition matrix element between the initial and final states of the emitter and ω is the frequency of

[a] Department of Physics, UMBC (University of Maryland, Baltimore County), 1000 Hilltop Circle, Baltimore, MD 21250 U.S.A. E-mail: mpelton@umbc.edu.

the emitted photon. A cavity increases the density of electromagnetic states at the frequencies of its optical modes, leading to an increase in the emission rate for emitters resonant with the cavity modes. For a narrow-linewidth emitter on resonance with a single-mode optical cavity, located at the maximum of the optical field in this mode and aligned with the polarization of the field, the emission rate is increased by the following Purcell factor compared to its emission rate in free space:[20]

$$F = \frac{3Q\lambda^3}{4\pi^2 V_o}, \quad (2)$$

where Q is the quality factor of the cavity, λ is the optical wavelength, and V_o is the cavity mode volume.

In this picture, a metal nanostructure can be seen as an optical resonator, and modification of spontaneous emission from materials next to the nanostructure is a result of localization of optical energy.[21] Compared to conventional optical cavities, plasmonic resonators have much lower quality factors; however, they can also have much smaller mode volumes, because they are not restricted by the diffraction limit.[22] The nanoscale mode volumes more than compensate for the small quality factors, so that plasmonic nanostructures have produced the largest observed enhancements of spontaneous emission.[21]

Strong coupling: Rabi splitting.

The cavity-QED description of plasmon-enhanced luminescence suggests the possibility of increasing the strength of plasmon-exciton coupling to the point where spontaneous emission into the plasmon modes is no longer irreversible, but energy is instead exchanged coherently back and forth between the exciton and plasmon before being radiated to free space or damped due to losses (see Figure 1a). The coherent oscillations of energy in the time domain (known as vacuum Rabi oscillations, see Figure 1b) correspond to the splitting of the emission peak into two (known as vacuum Rabi splitting, see Figure 1c).[23] The two peaks correspond to normal modes of the coupled plasmon-exciton system; that is, the new resonances correspond to hybrid plasmon-exciton states known as polaritons (or plexcitons). The

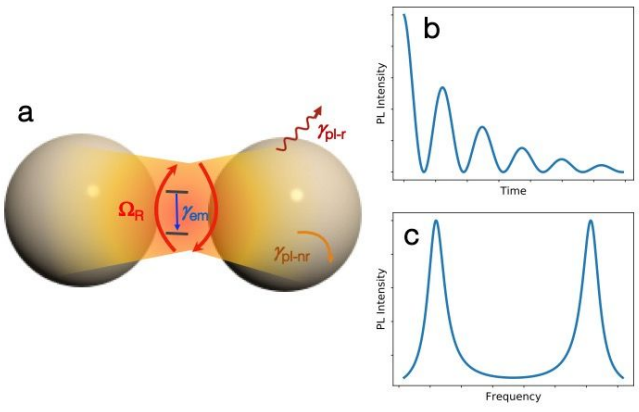

Figure 1: (a) Illustration of a strongly coupled plasmon-exciton system. The excitonic system undergoes dephasing and decay at a rate γ_{em}. The plasmonic system decays radiatively at a rate $\gamma_{pl\text{-}r}$ and non-radiatively at a rate $\gamma_{pl\text{-}nr}$, resulting in a total decay rate γ_{pl}. Energy oscillates between the plasmon and the exciton at the Rabi frequency Ω_R, as illustrated in **(b)**. These Rabi oscillations lead to splitting of the spectrum into hybrid modes, as illustrated in **(c)**.

formation of polaritons occurs in which is known as the strong-coupling regime of cavity QED, in contrast to the weak-coupling regime of modified spontaneous emission.

Strong coupling between an emitter and a plasmonic metal nanostructure can be modelled by treating the emitter as a two-level system and by considering a single resonant mode (or quasi-normal mode)[24] of the plasmonic nanostructure. Quantizing the plasmon field in terms of boson operators, $\hat{a}, \hat{a}^\dagger$, enables the system to be described in terms of the Jaynes-Cummings Hamiltonian:[25,26]

$$\hat{H} = \hbar\omega_{pl}\hat{a}^\dagger\hat{a} + \hbar\omega_{em}\hat{\sigma}^\dagger\hat{\sigma} + \hbar g(\hat{a}^\dagger\hat{\sigma} + \hat{\sigma}^\dagger\hat{a}), \quad (3)$$

where $\hat{\sigma}$ is the Pauli raising operator for the two-level system, ω_{pl} is the plasmon resonance frequency, ω_{em} is the emitter transition frequency, g is the coupling strength between the plasmon and the emitter, and damping and decoherence of the plasmon and the emitter have been ignored for the moment. The coupling strength is given by

$$g = \frac{2\vec{\mu}_{em}\cdot\vec{\mathcal{E}}_o}{\hbar}, \quad (4)$$

where $\vec{\mu}_{em}$ is the transition dipole matrix element of the emitter and $\vec{\mathcal{E}}_o$ is the local electric field produced by the plasmon at the location of the emitter.[27] For electromagnetic fields confined within a cavity with mode volume *V*, the maximum coupling strength (for an emitter located at the field maximum whose dipole moment is aligned with the polarization of the field) is

$$g = \frac{\mu_{em}}{\hbar}\sqrt{\frac{\hbar\omega_{pl}}{2V}}. \quad (5)$$

Diagonalization of the Hamiltonian in Eq. (3) gives the mode frequencies of the polaritons:

$$\omega_\pm = \frac{1}{2}(\omega_{pl} + \omega_{em}) \pm \Omega_R, \quad (6)$$

where the vacuum Rabi frequency is

$$\Omega_R = \sqrt{g^2 + 1/4(\omega_{pl} - \omega_{em})^2}. \quad (7)$$

Ω_R is the frequency at which energy oscillates between the plasmon and the emitter, as illustrated in Figure 1b.

Damping can be taken into account using the Heisenberg-Langevin approach, where the plasmon and emitter are each coupled to a reservoir of harmonic-oscillator modes.[28,29] Absorption spectra can be calculated directly from the resulting equations of motion using a Green's-function approach.[30,31] Equivalently, the system dynamics can be described using a Liouville, or master-equation, approach, with Lindblad operators used to describe the coupling of the plasmon and emitter to thermal reservoirs.[29,32,33,34,35,36] Scattering and absorption cross-sections can be calculated from either the Heisenberg-Langevin or the Liouville equations, by adding an external electric field, $\mathcal{E}$, that acts on the plasmon:

$$\hat{H}_d = -\mathcal{E}\hat{\mu}_{pl}, \quad (8)$$

where $\hat{\mu}_{pl} = d_{pl}(\hat{a} + \hat{a}^\dagger)$ is the plasmon dipole operator and d_{pl} is the plasmon dipole moment. Direct driving of the emitter by the external field can be neglected, because the emitter interacts much more weakly with light than does the plasmonic nanostructure. (Typically, the optical cross-section of an exciton is 3 – 4 orders of magnitude smaller than that of a 10 – 100 nm plasmonic metal nanoparticle.) The optical response can then be obtained by solving the equations of motion in either the time or frequency domain.

This analytical approach involves several assumptions. By treating the emitter as a two-level system, it ignores the complicated energy-level structure that is present in any quantum emitter. By treating the plasmon field in terms of the population of a single (quasi-)normal mode, it ignores additional modes that may overlap in frequency as well as any frequency dependence of the plasmon damping rate. Finally, it treats the emitter as a point dipole, ignoring any effects that arise as a result of field gradients across the spatial extent of the emitter. Despite the several simplifications involved, the model can nonetheless provide a quantitative treatment of experimental data, as we show below.

Solution of the quantum model requires substantial computational resources in order to account for all of the plasmon states that may be occupied. Significant speed-up can be obtained if the plasmon field can be approximated as classical, *i.e.*, if the effect of quantum fluctuations in the field can be neglected. In this case, the Heisenberg-Langevin or Liouville equations reduce to semiclassical Maxwell-Bloch equations,[37,38] provided these equations are written in the correct form.[29,39] We have verified that the predictions of the quantum and semiclassical models are nearly identical in the case of parameters relevant to plasmon-exciton coupling,[36] using the following form of the Maxwell-Bloch equations:[40]

$$\ddot{\mu}_{pl} + \gamma_{pl}\dot{\mu}_{pl} + \omega_{pl}^2\mu_{pl} = F_o + g(\omega_{pl}d_{pl}/d_{em})\mu_{em}, \quad (9)$$

$$\begin{cases} \dot{\rho}_1^{em} = \omega_{em}\rho_2^{em} - \gamma_2\rho_1^{em} \\ \dot{\rho}_2^{em} = -\omega_{em}\rho_1^{em} - (g/d_{pl})\mu_{pl}\rho_3^{em} - \gamma_2\rho_2^{em}, \\ \dot{\rho}_3^{em} = (g/d_{pl})\mu_{pl}\rho_2^{em} - \gamma_1(\rho_3^{em} + 1) \end{cases} \quad (10)$$

where d_{em} is the transition dipole moment of the emitter, γ_{pl} is the plasmon decay rate, γ_1 is the energy decay rate of the emitter, γ_2 is the dephasing rate of the emitter, $\hat{\rho}_{em}$ is the reduced density matrix of the emitter, $\rho_1^{em} = 2\,\Re[\rho_{01}]$, $\rho_2^{em} = -2\Im[\rho_{01}]$, $\rho_3^{em} = \rho_{11} - \rho_{00}$, and $F_o = 4\omega_{pl}d_{pl}^2\mathcal{E}$. Pure dephasing of the plasmon can be ignored, because it is slow compared to energy damping. The value of γ_1 must be taken as the value in the presence of the plasmonic metal nanostructure;[36] *i.e.*, the free-space decay rate multiplied by the Purcell factor in Eq. (2).

Differentiation of the first of Eq. (10) with respect to time and substitution of the second equation into the first gives $\ddot{\rho}_1^{em} = \omega_{em}\left[-\omega_{em}\rho_1^{em} - -(g/d_{pl})\mu_{pl}\rho_3^{em} - \gamma_2\rho_2^{em}\right] - \gamma_2\dot{\rho}_1^{em}$. In the case of the linear response (scattering or absorption) of the coupled system, we can make the further approximations that coherences between the ground and excited states of the emitter are negligible and that the population of the emitter remains nearly entirely in its ground state; *i.e.*, $\rho_3^{em} \approx -1$ and $\rho_2^{em} \ll 1$. Using $\mu_{em} = d_{em}\rho_1^{em}$, we obtain

$$\ddot{\mu}_{em} + \gamma_{em}\dot{\mu}_{em} + \omega_{em}^2\mu_{em} = g(\omega_{em}d_{em}/d_{pl})\mu_{pl}, \quad (11)$$

where we have assumed that dephasing of the emitter is much faster than energy decay, so the total emitter decay rate $\gamma_{em} \approx \gamma_2$. This last assumption will be valid for all experiments at or near room temperature.

Eqs. (9) and (11) describe a pair of coupled classical harmonic oscillators, with the displacement of each oscillator corresponding to the dipole moment of the plasmon and the exciton, respectively, and with the two oscillators coupled through the electromagnetic near field. The plasmon oscillator is driven by an external field, and the exciton oscillator is driven only through its coupling to the plasmon. This coupled-oscillator model provides a simple, intuitive picture of the coupled plasmon-emitter system.[41]

The coupled-oscillator equations can be readily solved in the frequency domain, in the absence of an external driving field, to give the normal-mode frequencies of the system. If we assume that coupling strength, damping rates, and detuning are small compared to the resonance frequencies $(g,\gamma_{em},\gamma_{pl},|\omega_{em} - \omega_{pl}| \ll \omega_{pl})$, then the normal-mode frequencies are

$$\omega_{\pm} = \frac{1}{2}(\omega_{pl} + \omega_{em}) - \frac{1}{4}i(\gamma_{pl} + \gamma_{em}) \pm \Omega_R, \quad (12)$$

where now

$$\Omega_R = \sqrt{g^2 + 1/4(\omega_{pl} - \omega_{em})^2 - 1/16(\gamma_{pl} - \gamma_{em})^2}. \quad (13)$$

Comparison to Eqs. (6) and (7) shows that the coupled-oscillator model gives the same results as the Jaynes-Cummings Hamiltonian in the limit of zero damping and dephasing. The normal modes are non-degenerate only if Ω_R is real. For $|\omega_{em} - \omega_{pl}| \ll \gamma_{pl}$, and for $\gamma_{em} < \gamma_{pl}$ (both fulfilled in all experiments that have been performed), this condition reduces to

$$g > \frac{1}{4}(\gamma_{pl} - \gamma_{em}). \quad (14)$$

This transition between the overdamped and the underdamped cases can be taken to represent the boundary between weak and strong coupling. However, it is more common to consider strong coupling to occur only when at least one complete Rabi oscillation occurs;[42] *i.e.*, when

$$g > \frac{1}{4}(\gamma_{pl} + \gamma_{em}). \quad (15)$$

In the following, we will use Eq. (15) to determine whether a system is in the strong-coupling regime. However, it is important to recognize that this does not represent a sharp threshold: there is no qualitative change in the behaviour of a coupled plasmon-emitter system as it crosses this boundary, and a case can be made for a strong-coupling condition that differs from this one by a numerical factor.

The coupled-oscillator equations can readily be generalized to the case where *N* emitters independently couple to a single plasmonic mode, each with a different coupling constant g_i.[41] In this case, the strong-coupling condition becomes

$$\sqrt{N}g_{rms} > \frac{1}{4}(\gamma_{pl} + \gamma_{em}), \quad (16)$$

where $g_{rms} = (1/N)\sum_{i=1}^{N} g_i$ and where we have assumed the same linewidth, γ_{em}, for all emitters.

Scattering spectra.

The coupled-oscillator equations can also be solved in the presence of a driving force to give scattering and absorption cross-sections. For a steady-state driving force at frequency ω, the solution is

$$\mu_{pl} = \frac{F_o(\omega_{em}^2 - \omega^2 - i\omega\gamma_{em})}{(\omega_{em}^2 - \omega^2 - i\omega\gamma_{em})(\omega_{pl}^2 - \omega^2 - i\omega\gamma_{pl}) - \omega_{em}\omega_{pl}g^2}. \quad (17)$$

The scattering cross-section is then given by[44]

$$\sigma_{scat}(\omega) \propto \omega^4|\mu_{pl}|^2. \quad (18)$$

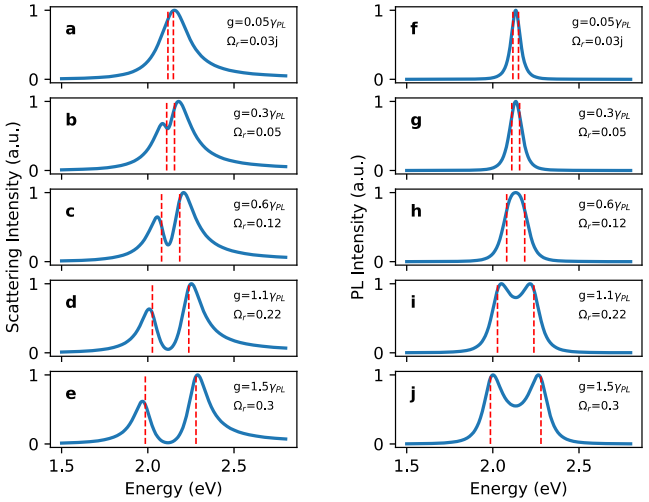

Figure 2: (a-e) Calculated scattering spectra for a coupled plasmon-emitter system with a plasmon resonance frequency ω_{sp} = 2.15 eV, emitter transition frequency ω_{em} = 2.12 eV, plasmon linewidth γ_{pl} = 0.2 eV, emitter linewidth γ_{em} = 0.06 eV, and varying coupling strength g, as indicated in the labels. Vertical dashed lines indicate the normal-mode frequencies for the coupled system. **(f-j)** Calculated luminescence spectra, for the same parameters as the corresponding scattering spectra.

Similar expressions can be obtained for the absorption and extinction cross-sections.[44] Spectra calculated according to Eqs. (17) and (18) are shown, for typical plasmon and exciton parameters, and for varying coupling strengths, in Figure 2a-e.

We note that, in a previous publication,[44] we used a version of the coupled-oscillator equations with different coupling terms:

$$\begin{cases} \ddot{\mu}_{pl} + \gamma_{pl}\dot{\mu}_{pl} + \omega_{pl}^2\mu_{pl} = F_o - g\dot{\mu}_{em} \\ \ddot{\mu}_{em} + \gamma_{em}\dot{\mu}_{em} + \omega_{em}^2\mu_{em} = g\dot{\mu}_{pl} \end{cases} \quad (19)$$

The coupling terms used in Eq. (9) and (11) are preferred, because they can be derived from quantum-mechanical models under classical, linear limits. However, if one uses the coupling terms in Eq. (19), the resulting steady-state solution differs only in the last term in the denominator:

$$\mu_{pl} = \frac{F_o(\omega_{em}^2 - \omega^2 - i\omega\gamma_{em})}{(\omega_{em}^2 - \omega^2 - i\omega\gamma_{em})(\omega_{pl}^2 - \omega^2 - i\omega\gamma_{pl}) - \omega^2 g^2}. \quad (20)$$

This will give nearly identical results to Eq. (17) as long as $g, \gamma_{em}, \gamma_{pl} \ll \omega$; this has been the case for all reported experimental results.

The success of the coupled-oscillator model makes it clear that the linear scattering or absorption response of a coupled plasmon-emitter system is classical and does not require quantum mechanics for its description. Indeed, scattering and absorption spectra can be calculated simply in terms of the classical electromagnetic response of the coupled system, provided the linear absorption and dispersion of the plasmonic metal nanoparticle and emitter are both taken into account.[43] Experimental dielectric functions of metals have been tabulated, and fits to these tabulated values are widely used in numerical solvers. The dielectric function of the emitter can be modelled as a Lorentzian with a center frequency ω_{em} and linewidth γ_{em} and with oscillator strength adjusted to match experimental absorption cross-sections.[44] With these values in hand, the scattering and absorption spectra can be calculated numerically using one of the widely employed methods for solving Maxwell's equations, such as the finite-difference time-domain (FDTD) method,[44,45] the discrete dipole approximation (DDA), [36,46] the finite-element (FE) method,[47] generalized Mie theory,[45,48,49] or transformation optics[50]. These numerical approaches can take into account the full geometry of the coupled system and no longer require the approximation of frequency-independent damping for the plasmon.

Luminescence spectra.

Although a fully classical treatment can describe quantitatively light scattered or absorbed by the coupled plasmon-emitter system, it cannot describe the light emitted by the system. Since spontaneous emission is a fundamentally quantum-mechanical phenomenon, arising from the interaction between the emitter and the surrounding electromagnetic vacuum, calculation of luminescence spectra requires a return to the Heisenberg-Langevin equations. These equations can be solved explicitly in the time domain for the initial condition of the emitter being in its excited state and the occupation of the plasmon mode being zero, using the Wigner-Weiskopf (or Markov) approximation that the dynamics of the system depend only on the current time.[51] This approximation is equivalent to the assumption that the reservoirs into which the plasmon and emitter decay are at zero temperature;[52] this is an excellent approximation for optical transitions at experimental temperatures.

Two different spectra can be calculated. The spectrum of light radiated by the emitter is calculated as the Fourier transform of the autocorrelation function for the excited state of the emitter:[51,52,53]

$$I_{em}(\omega) = \frac{\gamma_{em}}{2\pi}\left|\frac{1/2\gamma_{pl} - i(\omega - \omega_{pl})}{[1/4(\gamma_{pl} + \gamma_{em}) + i/2(\omega_{pl} - \omega_{em}) - i(\omega - \omega_{pl})]^2 + \Omega_R^2}\right|^2 \quad (21)$$

The spectrum of light radiated by the plasmon is calculated as the autocorrelation function for the plasmon occupation:

$$I_{pl}(\omega) = \frac{\gamma_{pl}}{\pi}\left|\frac{g/2}{[1/4(\gamma_{pl} + \gamma_{em}) + i/2(\omega_{pl} - \omega_{em}) - i(\omega - \omega_{pl})]^2 + \Omega_R^2}\right|^2 \quad (22)$$

Spectra calculated according to (21) are shown, for typical plasmon and exciton parameters, and for varying coupling strengths, in Figure 2f-j.

Intermediate coupling: Exciton-induced transparency.

As illustrated in Figure 2, as the coupling strength, g, increases, the scattering and luminescence spectra of the coupled plasmon-emitter system each evolve from a single peak, for $g \ll \gamma$, to a pair of well-defined peaks, for $g \gg \gamma$. Intermediate to these clear weak- and strong-coupling regimes, however, there is a range of values of g for which the luminescence spectrum displays only a single peak but two maxima are present in the scattering spectrum. It is thus clear that, in this intermediate-coupling regime, the two maxima in the scattering spectra do not arise from Rabi splitting and the formation of hybrid plasmon-exciton states. Rather, a dip forms in the scattering spectrum at ω_{em} due to destructive interference between the plasmon and emitter dipoles. This effect has been known for some time in cavity QED, and has been termed "dipole-induced transparency,"[54] in analogy to the phenomenon of electromagnetically-induced transparency.[55] In the case of plasmon-exciton coupling, it can be referred to more specifically as "exciton-induced transparency" (ExIT).[56]

The physical origin of this induced transparency can be understood by observing that the plasmon dipole moment, Eq. (17), can be written in the form

$$\frac{\mu_{pl}}{\mu_{pl}^{o}} = \frac{q+\epsilon}{q+i}, \tag{23}$$

where μ_{pl}^{o} is the plasmon dipole moment in the absence of the emitter and, in general, q and ϵ are complex parameters.[57,58] In the case of intermediate coupling and for emitter linewidth small compared to the plasmon linewidth, (*i.e.*, for $g \ll \gamma_{em} \ll \gamma_{pl}$),

$$\begin{cases} q \approx 2(\omega_{pl} - \omega_{em})/\gamma_{pl} \\ \epsilon \approx (\omega - \omega_{em})/\gamma_{pl} \end{cases}. \tag{24}$$

In this limit, the scattering cross-section can be written as

$$\frac{\sigma_{scat}}{\sigma_{scat}^{o}} = \frac{(q+\epsilon)^2}{1+\epsilon^2}. \tag{25}$$

This is the well-known Fano lineshape, with ϵ the reduced frequency and q the Fano asymmetry parameter.[59,60] The scattering spectrum in the intermediate-coupling regime can thus be understood as the result of Fano-like interference between a narrow emitter resonance and a broad, continuum-like plasmon resonance.

It is also informative to consider the case of resonant excitation with the plasmon and emitter also on resonance with one another, $\omega = \omega_{pl} = \omega_{em}$. In this case, the plasmon dipole moment, Eq. (17), can be written in the form

$$\frac{\mu_{pl}}{\mu_{pl}^{o}} = \frac{1}{1+C}, \tag{26}$$

where the cooperativity factor is defined as

$$C = g^2/(\gamma_{pl}\gamma_{em}). \tag{27}$$

The cooperativity is thus the only factor that determines the spectral response of the coupled system on resonance.[54] In particular, C determines the degree of induced transparency, and can thus be considered a figure of merit for the intermediate-coupling regime.

The quest for single-exciton strong coupling to plasmons

As Eq. (16) shows, the most straightforward route to reaching the strong-coupling regime is to increase the number of emitters coherently coupled to a single plasmon mode. The first reports of strong plasmon-exciton coupling thus involved macroscopic numbers of excitons, either in ensembles of molecules or extended semiconductor structures, coupled to propagating surface-plasmon polaritons on metal films.[61,62] There have been many subsequent studies that employed this same configuration,[63,64,65,66,67] although it is worth noting that the physics of this two-dimensional system is somewhat different from the physics of coupling to spatially localized plasmon resonances.[68] Additional experiments involved macroscopic numbers of excitons coupling to large numbers of localized surface plasmons, either in patterned metal films,[69,70,71,72,73] nanoparticle arrays,[74,75,76,77,78,79,80,81,82,83] or ensembles of nanoparticles.[84,85,86,87,88,89,90,91,92,93,94]

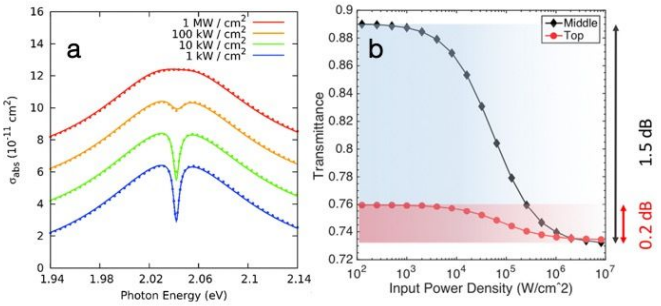

Figure 3: (a) Calculated absorption spectra for continuous-wave illumination of an assembly consisting of a single quantum dot between a pair of ellipsoidal gold nanoparticles, for various input power density. This figure has been reproduced from Ref. 36 with permission from the American Physical Society. **(b)** Calculated transmittance through a silicon waveguide as a function of input power density, with a single assembly on top of or embedded in the middle of the waveguide. This figure has been reproduced from Ref. 110 with permission from the Optical Society of America.

However, qualitatively different behaviour is expected and new applications are enabled if strong coupling can be achieved between a single exciton and a plasmon resonance. In particular, a strongly-coupled cavity-QED system with a single emitter is expected to exhibit a highly nonlinear response.[42] Systems with single self-assembled quantum dots (QDs) in photonic cavities have been used to demonstrate this nonlinearity[95] and to show that the state of a single QD can be used to control the amplitude, phase, and polarization of an optical signal, down to the single-photon level.[96,97,98,99] In addition, the polarization of a photon can be used to control the state of a single QD;[100] combining these functions enables all-optical switching[101] at the single-photon level.[102]

A significant limitation of these experiments, however, is that they require operation at cryogenic temperatures. The reason for this is that the diffraction limit restricts the mode volume, V, of a photonic cavity to be more than approximately $(\lambda/2)^3$, where λ is the wavelength of light inside the cavity. This, in turn, limits the maximum value of the coupling strength, g, according to Eq. (5). In order to achieve the high cooperativity that is required for these quantum-information applications, it is necessary to have low γ_{em} and γ_{pl}, according to Eq. (27). The cavity linewidth, γ_{pl}, can be made small in photonic cavities, which can have optical quality factors on the order of 10^5. The emitter linewidth, γ_{em}, on the other hand, can be made small only by cooling the system and reducing thermal dephasing.

Plasmonic metal nanostructures, by contrast, can confine optical fields to dimensions well below the diffraction limit,

enabling much higher values of *g*. Although a single plasmonic metal nanoparticle can already achieve sub-diffraction confinement, even stronger field confinement is achieved in the gap between a pair of closely spaced nanoparticles.[103,104] This localization occurs due to electrostatic coupling between the plasmons in the nanoparticles; the resulting coupled plasmon oscillation concentrates surface charge next to the gap, leading to fields that can be localized on the few-nanometer scale.[22,105] A similar degree of localization can be obtained for nanometer-scale gaps between a metal nanoparticle and a metal film;[106,107,108] in this case, the coupling can be thought of as occurring between the nanoparticle plasmon and its image dipole in the film. Coupling emitters to these gap plasmons thus has the potential to provide large coupling strengths and enable room-temperature strong coupling to single emitters, despite the large linewidths of plasmonic resonances.

Attempts to use coupled plasmon-exciton systems for quantum-information applications, however, will face the ultrafast damping of plasmons, which inevitably occurs on time scales of 10 – 100 fs.[109] It may be more realistic in the short run to consider plasmon-exciton coupling for classical information-processing applications, which can take advantage of the strong optical nonlinearities without being as sensitive to energy decay and dephasing. In particular, the nonlinearity provided by ExIT has the potential to occur at low energy densities, on ultrafast time scales, and on nanometer length scales, all the factors that are required for next-generation on-chip all-optical modulation.

In order to quantify the nonlinear response and assess this potential, it is necessary to go beyond the classical, linear treatment of the coupled plasmon-exciton system. It is possible to directly solve the quantum-mechanical Heisenberg-Langevin or Liouville equations, but an accurate description can be obtained more easily by solving the semiclassical Maxwell-Bloch equations (9) and (11). Figure 3a shows the results of these calculations for a model system of a single colloidal QD between a pair of ellipsoidal gold nanoparticles under continuous-wave illumination.[36] As the incident optical intensity increases, the ExIT dip disappears, due to saturation of the QD transition.[30] This saturation-induced nonlinearity is the only nonlinearity active in these calculations; in particular, the nonlinear Fano effects predicted in some calculations[27,38,56] are not present in this formalism.[39]

The nonlinearity corresponding to the disappearance of the transparency dip occurs at moderate power densities; however, since the physical dimensions of the coupled nanoparticle assembly are so small, the total power required for modulation is also very small. As well as enabling all-optical modulation, this nonlinearity has the potential to enable more advanced forms of optical information processing, such as neuromorphic computing.[110] Neural networks are composed of artificial "neurons" that combine multiple incoming signals through weighted addition, apply a nonlinear activation function to the weighted sum, and transmit the resulting signal to multiple destination neurons. A coupled plasmon-exciton system can provide an all-optical nonlinear activation function, as illustrated in Figure 3b.

Both the classical and potential quantum-mechanical information-processing applications of coupled plasmon-exciton systems rely on a strong ExIT dip, and thus require a large cooperativity, *C*. Achieving a value of $C > 1$ is often taken as a minimum condition for single-photon nonlinearities. However, like the strong-coupling threshold given in Eq. (15), this does not represent a firm dividing line between two qualitatively different regimes, but rather is a rule of thumb to help evaluate the promise of a particular configuration.

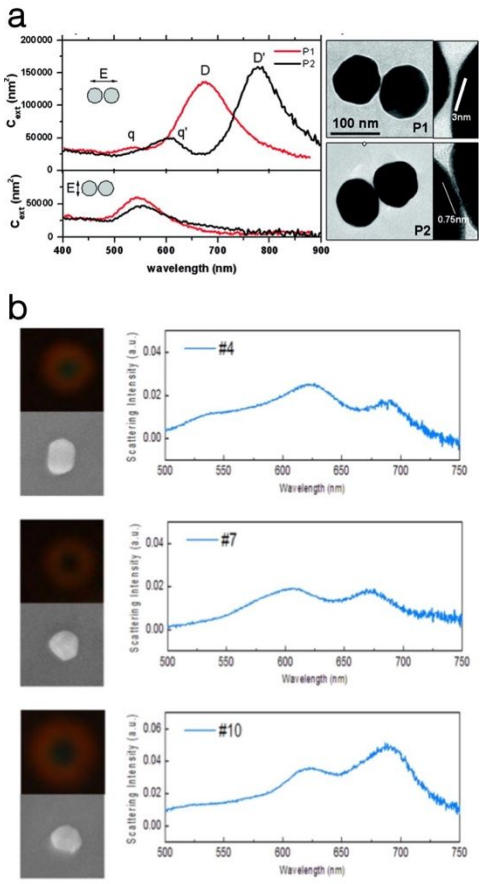

Figure 4: (a) Left figures show measured extinction cross-sections for two pairs of gold nanoparticles, for two different polarizations of incident light. D and q label dipolar and quadrupolar plasmon resonances. Right figures show transmission-electron-microscope images of the measured nanoparticle pairs. This figure has been reproduced from Ref. 114 with permission from the American Chemical Society. **(b)** Right figures show measured scattering spectra for single quasi-spherical gold nanoparticles on a flat gold film. Left images show dark-field optical microscope and scanning electron microscope images of the measured particles. This figure has been reproduced from Ref. 112 with permission from the American Chemical Society.

Distinguishing intermediate and strong coupling

Analysis of scattering lineshape.

Experiments involving propagating surface-plasmon polaritons or ensembles of plasmonic metal nanostructures often involve measurements of absorption or extinction. Experiments with single metal nanostructures, by contrast, most commonly involve dark-field scattering measurements, because these provide the most experimentally straightforward way to obtain the spectral response of individual nanostructures.[22,111] A scattering spectrum with two maxima has often been taken to be a signature of strong coupling, and the frequency separation between the two maxima has often been taken to be equal to the coupling strength, *g*, or the Rabi frequency, Ω_R. However, as Figure 2 illustrates, interference effects can produce a dip in the scattering spectrum,

and thus two maxima, when g is below the strong-coupling threshold. Moreover, even in the strong-coupling regime, the combination of ExIT and Rabi splitting mean that the maxima in the scattering spectrum are not located at the normal-mode frequencies; only for $g \gg \gamma_{sp}$ does the peak separation become a good approximation of the coupling strength.

Rather, in order to determine the coupling strength quantitatively and distinguish strong coupling from intermediate coupling on the basis of a scattering measurement, it is necessary to fit the full scattering lineshape to the expected spectrum, given by Eqs. (17) and (18).

Measurement of photoluminescence spectra.

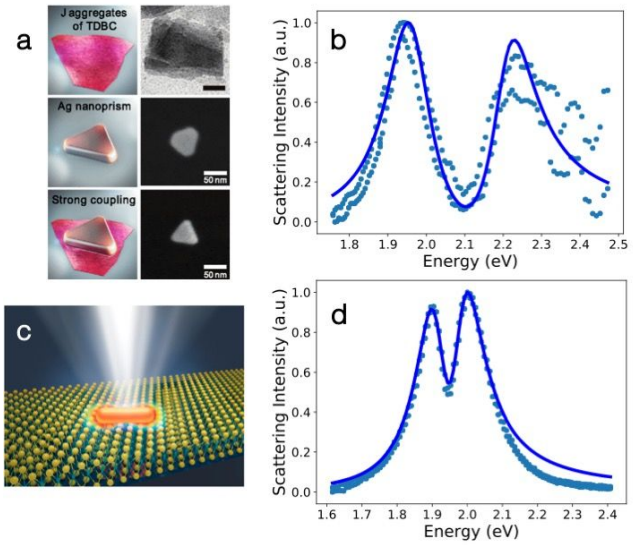

Figure 5: (a) Illustration and scanning-electron microscope images of the preparation of a silver nanoprism coupled to a layer of J-aggregates. This figure has been reproduced from Ref. 117 with permission from the American Physical Society. **(b)** Measured scattering spectrum (points) from a the nanoprism J-aggregate system (from Fig. 1c of Ref. 117) and fit to coupled-oscillator model (line). **(c)** Illustration of a single gold nanorod coupled to a layer of WS_2. This figure has been reproduced from Ref. 125 with permission from the Americal Chemical Society. **(d)** Data for the nanorod-WS_2 system (from Fig. 1d of Ref. 125, bottom curve) and fit.

ExIT is an interference effect that results from the coherence that is set up by the external driving field. It thus does not affect luminescence, which does not involve an external field. Therefore, as can be seen in Figure 2, luminescence spectra provide the qualitative distinction between intermediate and strong coupling that is not provided by scattering spectra: the presence of two peaks in a luminescence spectrum is a definitive signature of strong coupling.[46]

This qualitative signature of strong coupling can also avoid mistaking other phenomena that can lead to two peaks in the scattering spectrum for strong coupling. For example, the nanostructures that can be synthesized or fabricated experimentally usually do not have the simple geometries that are assumed theoretically, but instead have surface roughness, grain boundaries, and facets. When non-ideal nanoparticles are used to form gap plasmons, the asymmetries in their structures can lead to multiple coupled-plasmon modes; these modes, in turn, can undergo Fano-like interference with one another that resembles interference between a plasmon mode and an excitonic transition. Figure 4b illustrates this for the case of quasi-spherical gold nanoparticles on a gold film.[112] In addition, multiple peaks can show up in the scattering spectrum from even an ideal pair of coupled metal nanoparticles, if the gap between the particles is on the scale of 1 nm or less (corresponding to typical molecular dimensions).[113,114] As illustrated experimentally in Figure 4a, the additional peaks arise from quadrupolar or higher-order multipolar modes in the coupled-plasmon system.

It has been proposed that absorption spectra can also avoid the ambiguities of ExIT and provide a qualitative signature of strong plasmon-exciton coupling.[46] However, the small absorption cross-sections of typical plasmonic nanostructures means that measuring the absorption of a single nanostructure is challenging and requires specialized techniques.[22,111] Provided the exciton involved emits light with a reasonable efficiency, then, measurement of a photoluminescence spectrum is the most experimentally practical way to qualitatively distinguish strong and weak coupling.

On the other hand, it can be difficult to quantitatively determine coupling strengths from luminescence spectra. The simple theory used to derive Eqs. (21) and (22) gives formulas for the spectrum emitted by the exciton and the spectrum emitted by the plasmon. In conventional cavity QED experiments, these two spectra can be isolated because of their nearly orthogonal radiation directions. For plasmon-exciton coupling, on the other hand, the radiation patterns are complex and overlapping. Although typical experimental configurations tend to collect primarily light radiated by the plasmon, the measured spectrum is a non-trivial combination of light radiated by both components of the coupled system. Quantitatively comparing theory and experiment thus requires a challenging numerical simulation. A more practical experimental procedure is thus to measure both scattering and luminescence, using the luminescence spectrum to provide a qualitative signature of strong coupling that eliminates any potential ambiguities, and fitting the scattering spectrum to quantitatively determine coupling strength.[47]

Critical review of published data

Coupling of multiple excitons to single plasmonic nanoparticles.

We have advocated above for the use of lineshape analysis (*i.e.* fitting) according to the coupled-oscillator model to determine coupling strengths in coupled plasmon-exciton systems. Although this method has been adopted by some authors, other have used different methods with varying degrees of rigorous justification. In order to provide a review of the literature in which all results are compared on equal footing, we have re-analyzed published data by fitting reported scattering spectra to Eqs. (17) and (18) and reported photoluminescence spectra to Eq. (22). Since our focus here is on the quest for strong coupling between single excitons and single plasmons, we consider only papers where measurements were made on single plasmonic nanostructures.

We extracted data from published figures of scattering and PL spectra using GetData Graph Digitizer (version 2.26). Fitting was performed using a nonlinear least-squares algorithm. When spectra for the isolated emitters or plasmon resonances were reported, we fit them separately to obtain corresponding frequencies and linewidths; when these spectra were not reported, we used values given in the text of the papers, when available. Fitted frequencies and linewidths for the coupled systems were constrained to be close to these known values.

Table 1 summarizes results for experiments in which multiple excitons were coupled to a single plasmonic nanostructure. In

most publications, several spectra were reported, for different nanostructures or under different conditions; the table reports the fitted parameters for the case that gave the largest value of the coupling strength, *g*. The table highlights cases where photoluminescence spectra were measured, providing a qualitative verification of strong coupling. Also highlighted are cases for which the strong-coupling criterion, Eq. (15), is satisfied. We reiterate that this criterion should be considered only a rule of thumb to distinguish between the intermediate- and strong-coupling regimes, and not an abrupt threshold; more important are the quantitative ratios of coupling strength to linewidths.

Table 1: Fitting results for published data on coupling of multiple emitters to single plasmonic nanostructures. For each reference, the indicated figure gave the largest value for the coupling strength *g*. Green highlighting indicates references for which photoluminescence (PL) was measured and references for which the strong-coupling criterion is fulfilled.

Ref.	Figure	PL?	*g* (eV)	$4g/(\gamma_{pl}+\gamma_{em})$
115	2a, pink line	No	0.30	2.84
116	4b	No	0.12	1.57
121	2a1	No	0.24	2.73
117	1c	No	0.25	3.51
119	2a, "50 nm"	No	0.09	1.37
132	2a, bottom line	No	0.16	1.15
131	4e	No	0.12	1.94
118	1	Yes	0.31	4.30
125	3a, purple line	No	0.10	1.92
120	4aVI	No	0.15	2.04
	4aI		0.06	1.08
126	2d, "-4V"	No	0.05	0.96
122	1d	No	0.13	1.90
127	2b	No	0.07	0.92
128	2a, "2.80"	No	0.07	1.84
129	3c, "10 nm"	No	0.06	1.27
124	3e	Yes	0.15	1.54
123	2c	No	0.11	1.27

The earliest publication in this table, Ref 115, reported results for J-aggregates deposited on top of microfabricated pairs of gold disks. J-aggregates have been popular molecular systems for demonstrating strong coupling, because the aggregates have narrow excitonic linewidths and large transition dipole moments.

Similar results were reported shortly afterwards, in Ref. 116, for J-aggregates on top of a silver nanorod. The same group followed up with measurements of J-aggregates on top of a silver triangular nanoprism (see Figure 5a-b),[117] for which considerably higher coupling strengths were obtained. Later measurements by the same group on an equivalent system included measurements of photoluminescence,[118] providing the first verification of this type that strong coupling was indeed occurring at the single particle level. We note, however, that fits of the photoluminescence spectra from this paper do not give the same coupling strengths as fits of the scattering spectra. In the paper, this discrepancy was discussed in terms of the possibility that the

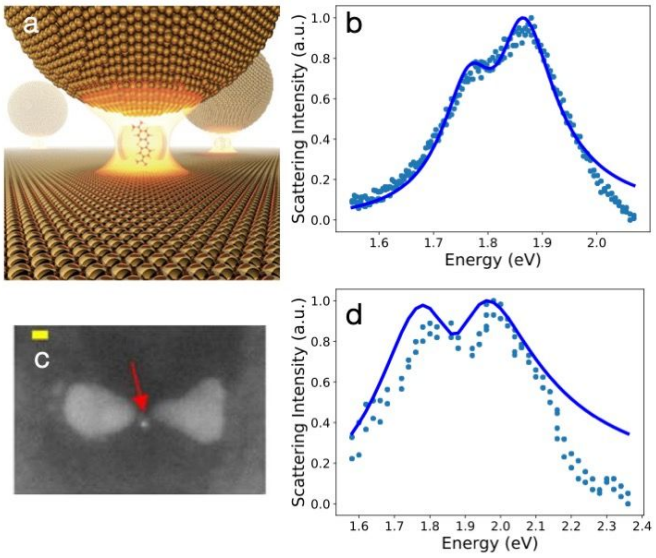

Figure 6: (a) Illustration of a single molecule in the gap between a gold nanosphere and a gold film. This figure has been reproduced from Ref. 131 with permission from Springer Nature. **(b)** Data (points) for the molecule / gap-plasmon system (from Fig. 4c of Ref. 131) and fit to a coupled-oscillator model (line). **(c)** Scanning-electron-microscope image of a single colloidal quantum dot in the gap of a gold bowtie nanoantenna. This figure has been reproduced from Ref. 132 with permission from Springer Nature. **(d)** Data for the quantum-dot / bowtie system (from Fig. 2 of Ref. 132, top curve) and fit.

higher-energy peak in the luminescence spectrum arises from uncoupled excitonic states, but this explanation is not quantitatively consistent with the measured spectra. More likely, the discrepancy arises because of the ambiguity, discussed above, in determining whether the measured spectrum corresponds to light emitted by the plasmon, the exciton, or both. The parameters reported in Table 1 are thus obtained by fitting scattering spectra.

Later experiments have also employed J-aggregates. In Ref. 119, greater control over the plasmon-exciton coupling was obtained by deterministically placing J-aggregates in the gap between two gold nanoparticles using DNA origami. In Ref. 120, cuboidal silver nanoparticles were coated with J-aggregates. In this experiment, the concentration of J-aggregates was reduced to the point where the average number of molecules coupled to a single nanoparticle was expected to be less than one. However, there was no direct determination of the number of molecules involved in a particular measurement; we therefore include this paper in the category of multiple excitons coupling to a single nanostructure. Reported in Table 1 are fitting results both for the case with largest *g* and for the case where the estimated number of molecules per metal nanoparticle is 0.7.

As well as the experiments involving J-aggregates, several others have focused on molecules coupled to gap plasmons. Ref. 121 reports results for molecules in the gap between a pair of silver nanoparticles. Ref. 122 reports results for molecules in the gap between a gold nanocube and a gold film, and Ref. 123 for molecules in the gap between a silver nanocube and a silver film. Ref. 124 reports results for molecules in the gap between a quasi-spherical gold nanoparticle and a gold film. Although Refs. 121 and 124 discuss their results in terms of single-molecule strong coupling, no direct evidence is provided that single molecules are involved.

Ref. 124 also reports photoluminescence spectra; fitting these spectra again gives coupling strengths that are different from those obtained by fitting the scattering spectra. This may again be due to the difficulty in assigning the emission to the exciton or the plasmon, although the authors of the paper also point out that the wavelength of the luminescence spectrum in the case of strong coupling to plasmons does not correspond to the wavelength of the luminescence for the bare dye molecules.

Finally, several authors have studied strong coupling between individual plasmonic metal nanostructures and excitons in two-dimensional transition metal dichalcogenides. Ref. 125 reported results for a gold nanorod on top of WS_2. (See Figure 5c-d.) Ref. 126 reported results for a gold nanodisk on top of MoS_2, Ref. 127 for a triangular gold nanoprism on top of WS_2, and Ref. 128 for a gold bipyramids on top WSe_2 layers. Ref. 129 employed gap plasmons, reporting results for WSe_2 layers between a silver nanocube and a gold film.

Coupling of single excitons to single plasmonic nanoparticles.

Table 2 summarizes results for experiments in which a single exciton was coupled to a single plasmonic nanostructure. As well as the values reported in Table 1, this table reports the cooperativity, *C*. Highlighted in the table are results for which $C > 1$; like the strong-coupling criterion, this should be taken as a suggestive rule of thumb, rather than a firm boundary between two different regions.

Table 2: Fitting results for published data on coupling of single emitters to single plasmonic nanostructures. For each reference, the indicated figure gave the largest value for the coupling strength *g*. Green highlighting indicates references for which photoluminescence (PL) was measured, references for which the strong-coupling criterion is fulfilled, and references for which the cooperativity, *C*, exceeds 1.

Ref.	Figure	PL?	*g* (eV)	$4g/(\gamma_{pl}+\gamma_{em})$	*C*
130	3d, "30 degrees"	No	0.12	0.80	0.2
131	4c	No	0.08	0.92	0.5
132	2a, top line	No	0.13	1.37	0.3
133	1cII	No	0.03	0.80	0.5
134	1, top left	Yes	0.12	3.01*	3.7*
			0.05	1.38*	0.6*
47	5a	Yes	0.23	3.68	3.5

Nearly all strong-coupling experiments with single excitons involve gap plasmons, because of their ability to confine fields to smaller volumes than isolated metal nanoparticles. The only exception is the earliest paper in the table, Ref. 130, where an AFM tip was used to place a single QD next to a single quasi-spherical gold nanoparticle and intermediate coupling was observed.

Ref. 131 reported measurements on molecules between a quasi-spherical gold nanoparticle and a gold film. (See Figure 6a-b.) The cases for which single molecules were involved were determined based on the measured coupling strengths and comparison to theory. We note, however, that the coupling strengths were obtained by fitting measured results to a sum of two peaks; we obtain different values by fitting to the coupled-oscillator model. Results that correspond to multiple molecules are reported in Table 1; we note that we were able to obtain good fits to the coupled-oscillator model for only some of the reported spectra.

Ref. 132 reported results for a single QD in the gap between a tip-to-tip pair of triangular gold nanoprisms, referred to as a bowtie nanoantenna. (See Figure 6c-d). The QDs were imaged by scanning electron microscopy, enabling a direct determination of the number of QDs involved in coupling; results with multiple QDs are reported in Table 1.

Ref. 133 reported results for single molecules in the gap between a silver scanning-probe tip and a silver surface. In this case, individual molecules were directly identified by STM imaging, and intermediate coupling was observed.

By contrast, strong coupling was reported in another scanning-probe experiment, using a single QD as the excitonic system and a gap fabricated on the end of a gold tip as the plasmonic probe.[134] Single QDs were identified by AFM imaging. Photoluminescence was measured, and an unexpected four-peak spectrum was observed. The authors attributed this to emission from charged and uncharged QD states: the two inner peaks were interpreted as arising from a charged exciton coupled to the plasmon, and the two outer peaks were interpreted as arising from a neutral exciton coupled to the plasmon. The values in Table 2 are determined by taking this interpretation at face value. We note, however, that there does not appear to be independent evidence supporting this interpretation; moreover, fitting the data in this way requires using QD linewidths that are outside of the range that would typically be expected. Because of this ambiguity, the fitted values are labelled with asterisks in Table 2.

A single QD was coupled to the gap plasmon between a quasi-spherical gold nanoparticle and a gold film in Ref. 47. In this case, both scattering and photoluminescence were measured. As for the previous papers discussed above, fits to the scattering and luminescence spectra give different coupling strengths; because of the ambiguity in interpreting luminescence spectra, values in Table 2 are from the fits to scattering spectra.

Concluding remarks

Re-analysis of published results shows that strong coupling has been clearly demonstrated in several cases when multiple excitons have been coupled to single plasmonic nanostructures. On the other hand, there have been only two unambiguous demonstrations of strong coupling between single excitons and single plasmonic metal nanostructures, and only one of those showed high cooperativity. In this case,[47] random chance was relied upon in order to place a QD in the gap between a metal nanoparticle and a metal film, and the fraction of structures that exhibited strong coupling or high cooperativity was very low. There is thus a need to develop synthesis and fabrication procedures that can, with high yield, produce devices that clearly show single-exciton / single-plasmon strong coupling.

There is also a need to better model the photoluminescence spectra from these coupled structures. In all the cases where both scattering and luminescence spectra were measured, fits to simple models do not result in the same fitted coupling strength. This is most likely due to the fact that the emission from the coupled system cannot be ascribed exclusively to the exciton or the plasmon but is a combination of the two that depends on the detailed radiation pattern of the system and the experimental detection geometry. Models that allow the calculation of the luminescence spectrum for an arbitrary detector position have been articulated,[135] and further

development of these models will allow for quantitative comparison between theory and experiment. Another promising theoretical direction is the development of models that go beyond the point-dipole approximation for the excitonic system and take into account the variation in the confined electromagnetic field across the dimensions of the emitter.[136,137,138]

In many cases, however, the simple, analytical models reviewed here allow for quantitative analysis of experimental data and unambiguous determination of coupling strengths. The same approach should be directly applicable to other strongly coupled plasmonic systems, such as coupling at infrared frequencies between plasmons and molecular vibrations.[139,140,141] We thus hope that this review will help researchers adopt a uniform method of reporting and analysing results in this rapidly developing field.

Conflicts of interest

There are no conflicts to declare.

Acknowledgements

We thank Molly May for assistance with figures. M.P. thanks Maxim Sukharev and David Masiello for helpful discussions. This work was supported in part by the National Institute of Standards and Technology under award number 70NANB18H282.

References

[1] F. Marquier, C. Sauvan, and J.-J. Greffet, *ACS Photonics*, 2017, **4**, 2091 – 2101.
[2] D. G. Baranov *et al.*, *ACS Photonics*, 2017, **5**, 24 – 42.
[3] A. J. Moilanen, T. K. Hakala, and P. Törmä, *ACS Photonics*, 2017, **5**, 54 – 64.
[4] G. Haran and L. Chuntonov, *Chem. Rev.*, 2018, **118**, 5539 – 5580.
[5] K. H. Drexhage, *J. Luminesc.*, 1970, **1**, 683 – 701.
[6] K. H. Drexhage, *Prog. Opt.*, 1974, **12**, 164 – 232.
[7] D. L. Jeanmaire and R. P. van Duyne, *J. Electroanal. Chem.*, 1977, **84**, 1 – 20.
[8] M. G. Albrecht and J. A. Creighton, *J. Am. Chem. Soc.*, 1977, **99**, 5215 – 5217.
[9] M. Moskovits, *Rev. Mod. Phys*., 1985, **57**, 783 – 826.
[10] A. M. Glass *et al., Opt. Lett.*, 1980, **5**, 368 – 370.
[11] G. Ritchie and E. Burstein, *Phys. Rev. B*, 1981, **24**, 4843 – 4846.
[12] A. Wokaun *et al., J. Chem. Phys.*, 1983, **79**, 509 – 514.
[13] A. Leitner *et al., Appl. Phys. B*, 1985, **36**, 105 – 109.
[14] P. Bharadwaj *et al., Adv. Opt. Photon.*, 2009, **1**, 438 – 483.
[15] J. Wessel, *J. Opt. Soc. Am. B*, 1985, **2**, 1538 – 1541.
[16] U. Ch. Fischer and D. W. Pohl, *Phys. Rev. Lett.*, 1989, **62**, 458 – 461.
[17] P. Goy *et al., Phys. Rev. Lett.*, 1983, **50**, 1903 – 1906.
[18] D. J. Heinzen *et al., Phys. Rev. Lett.*, 1987, **58**, 1320 – 1323.
[19] C. Cohen-Tannoudji, B. Liu, F. Laloë, *Quantum Mechanics, Vol. 2*, John Wiley & Sons, New York, 1977.
[20] E. M. Purcell, *Phys. Rev.*, 1946, **69**, 681.
[21] M. Pelton, *Nat. Photon.*, 2015, **9**, 427 – 435.
[22] M. Pelton and G. Bryant, *Introduction to Metal-Nanoparticle Plasmonics*, John Wiley & Sons, Hoboken, 2013.
[23] J. J. Sanchez-Mondragon *et al., Phys. Rev. Lett.*, 1983, **51**, 550 – 553.
[24] C. Sauvan *et al*., *Phys. Rev. Lett.*, 2013, **100**, 237401.
[25] E. T. Jaynes and F. W. Cummings, *Proc. IEEE*, 1963, **51**, 89 – 109.
[26] J. M. Raimond *et al., Rev. Mod. Phys.,* 2001, **73**, 565 – 582.
[27] W. Zhang *et al., Phys. Rev. Lett.,* 2006, **97**, 146804.
[28] M. O. Scully and M. S. Zubairy, *Quantum Optics*, Cambridge University Press, Cambridge, U.K., 1997.
[29] E. Waks and D. Sridharan, *Phys. Rev. A*, 2010, **82**, 043845.
[30] A. Manjavacas *et al., Nano Lett.,* 2011, **11**, 2318 – 2323.
[31] A. Delga *et al*., *Phys. Rev. Lett.*, 2014, **112**, 253601.
[32] D. F. Walls and G. J. Millburn, *Quantum Optics, 2nd Ed.*, Springer-Verlag, Berlin, 2008.
[33] A. Truegler and U. Hohenester, *Phys. Rev. B*, 2008, **77**, 115403.
[34] A. Ridolfo *et al*., *Phys. Rev. Lett.*, 2010, **105**, 263601.
[35] T. Hümmer *et al*., *Phys. Rev. B*, 2013, **87**, 115419.
[36] R. A. Shah *et al., Phys. Rev. B,* 2013, **88**, 075411.
[37] M.-T. Cheng *et al.*, *Opt. Lett.*, 2007, **32**, 2125 – 2127.
[38] R. D. Artuso and G. W. Bryant, 2008, *Nano Lett.*, **8**, 2106 – 2111.
[39] X.-W. Chen, V. Sandoghdar, and M. Agio, *Phys. Rev. Lett.*, 2013, **110**, 153605.
[40] R. W. Zikolkowski *et al., Phys. Rev. A*, 1995, **52**, 3082 – 3094.
[41] S. Rudin and T. L. Reinecke*, Phys. Rev. B*, 1999, **59**, 10227 – 10233.
[42] G. Khitrova *et al., Nat. Phys.,* 2006, **2**, 81 – 90.
[43] Y. Zhu *et al., Phys. Rev. Lett.*, 1990, **64**, 2499 – 2502.
[44] X. Wu *et al., Opt. Express,* 2010, **18**, 23633 – 23645.
[45] T. S. Antosiewicz, S. P. Apell, and T. Shegai, *ACS Photonics*, 2014, **1**, 454 – 463.
[46] N. Murata, R. Hata, and H. Ishihara, *J. Phys. Chem. C*, 2015, **119**, 25493 – 25498.
[47] H. Leng *et al.*, *Nat. Comms.*, 2018, **9**, 4012.
[48] S. Savasta *et al.*, *ACS Nano*, 2010, **4**, 6369 – 6376.
[49] A. Cacciola *et al.*, *ACS Nano*, 2014, **8**, 11483 – 11492.
[50] R.-Q. Li *et al*., *Phys. Rev. Lett.*, 2016, **117**, 107401.
[51] G. Cui and M. G. Raymer, *Phys. Rev. A*, 2006, **73**, 053807.
[52] F. P. Laussy, E. del Valle, and C. Tejedor, *Phys. Rev. B*, 2009, **79**, 235325.
[53] G. Cui and M. G. Raymer, *Phys. Rev. A*, 2008, **78**, 049904.
[54] E. Waks and J. Vuckovic, *Phys. Rev. Lett.,* 2006, **96**, 153601.
[55] K.-J. Boller, A. Imamoglu, and S. E. Harris, *Phys. Rev. Lett.*, 1991, **66**, 2593 – 2596.
[56] R. A. Artuso and G. W. Bryant, *Phys. Rev. B*, 2010, **82**, 195419.
[57] N. Thakkar *et al., Nano Lett.*, 2017, **17,** 6927 – 6934.
[58] J. Yang *et al., Phys. Rev. X*, 2015, **5**, 021008.
[59] U. Fano, *Phys. Rev.*, 1961, **124**, 1866 – 1878.
[60] J.-P. Connerade and A. M. Lane, *Rep. Prog. Phys.*, **51**, 1439 – 1478.
[61] I. Pockrand, A. Brillante, and D. Möbius, *J. Chem. Phys.*, 1982, **77**, 6289-6295.
[62] J. Bellessa *et al*., *Phys. Rev. Lett.*, 2004, **93**, 036404.
[63] T. K. Hakala *et al.*, *Phys. Rev. Lett.,* 2009, **103**, 053602.
[64] D. E. Gómez *et al*., *Nano Lett.*, 2009, **10**, 274 – 278.
[65] L. Stern, M. Grajower, and U. Levy, *Nat. Comms.*, 2014, **5**, 4865.
[66] G. Beane *et al*., *J. Phys. Chem. Lett*., 2018, **9**, 1676 – 1681.
[67] Q. Shang *et al.*, *Nano Lett*., 2018, **18**, 3335 – 3343.
[68] P. Törmä and W. L. Barnes, *Rep. Prog. Phys.*, 2015, **78**, 013901.
[69] J. Dintinger *et al*., *Phys. Rev. B*, 2005, **71**, 035424.

[70] Y. Sugawara *et al*., *Phys. Rev. Lett.*, 2006, **97**, 266808.
[71] P. Vasa *et al.*, *Phys. Rev. Lett.*, 2008, **101**, 116801.
[72] P. Vasa *et al.*, *ACS Nano*., 2010, **4**, 7559 – 7565.
[73] P. Vasa *et al*., *Nat. Photon.*, 2013, **7**, 128 – 132.
[74] J. Bellessa *et al*., *Phys. Rev. B*, 2009, **80**, 033303.
[75] A. I. Väkeväinen *et al*., *Nano Lett.*, 2014, **14**, 1721 – 1727.
[76] L. Shi *et al*., *Phys. Rev. Lett.*, 2014, **112**, 153002.
[77] B. Lee *et al.*, *Nano Lett.*, 2015, **15**, 3646 – 3653.
[78] E. Eizner *et al*., *Nano Lett*., 2015, **15**, 6215 – 6221.
[79] W. Liu *et al*., *Nano Lett.*, 2016, **16**, 1262 – 1269.
[80] S. Wang *et al*., *Nano Lett.*, 2016, **16**, 4368 – 4374.
[81] B. Lee *et al*., *Nano Lett*., 2017, **17**, 4541 – 4547.
[82] I. Abid *et al*., *ACS Photonics*, 2017, **4**, 1653 – 1660.
[83] E. Eizner *et al*., *Nano Lett.*, 2017, **17**, 7675 – 7683.
[84] G. P. Wiederrecht, G. A. Wurtz, and J. Hranisavljevic, *Nano Lett.*, 2004, **4**, 2121 – 2125.
[85] G. L. Liu *et al.*, *Nat. Methods*, 2007, **4**, 1015 – 1017.
[86] N. T. Fofand *et al.*, *Nano Lett.,* 2008, **8**, 3481 – 3487.
[87] A. Yoshida, N. Uchida, and N. Kometani, *Langmuir*, 2009, **25**, 11802 – 11807.
[88] D. D. Lekeufack *et al*., *Appl. Phys. Lett.*, 2010, **96**, 253107.
[89] S. Balci, *Opt. Lett*., 2013, **38**, 4498 – 4501.
[90] S. Balci *et al*., *Appl. Phys. Lett.*, 2014, **105**, 051105.
[91] D. Melnikau *et al*., *J. Phys. Chem. Lett.*, 2016, **7**, 354 – 362.
[92] N. Zhou *et al*., *ACS Nano*, 2016, **10**, 4154 – 4163.
[93] S. Balci *et al*., *ACS Photonics*, 2016, **3**, 2010 – 2016.
[94] F. Stete *et al*., *ACS Photonics*, 2017, **4**, 1660 – 1676.
[95] K. Srinvasan and O. Painter, *Nature*, 2007, **450**, 862 – 865.
[96] D. Englund *et al*., *Nature*, 2007, **450**, 857 – 861.
[97] I. Fushman *et al*., *Science*, 2008, **320**, 769 – 772.
[98] H. Kim *et al*., *Nat. Photon*., 2013, **7**, 373 – 377.
[99] C. Arnold *et al*., *Nat. Comms*., 2015, **6**, 6236.
[100] S. Sun *et al*., *Nat. Nanotech*., 2016, **11**, 539 – 544.
[101] T. Volz *et al*., *Nat. Photon.*, 2012, **6**, 605 – 609.
[102] S. Sun *et al*., *Science*, 2018, **361**, 57 – 60.
[103] H. Xu *et al*., *Phys. Rev. Lett.*, 1999, **83**, 4357 – 4360.
[104] A. M. Michaels, J. Jiang, and L. Brus, *J. Phys. Chem. B*., 2000, **104**, 11965 – 11971.
[105] N. J. Halas *et al*., *Chem. Rev.*, 2011, **111**, 3913 – 3961.
[106] G. Lévêque and O. J. F. Martin, *Opt. Express*, 2006, **14**, 9971 – 9981.
[107] P. Nordlander and F. Le, *Appl. Phys. B*, 2006, **84**, 35 – 41.
[108] J. J. Baumberg *et al*., *Nat. Mater*., 2019, DOI: 10.1038/s41563-019-0290-y
[109] J. B. Khurgin, *Nat. Nanotech*., 2015, **10**, 2 – 6.
[110] M. Miscuglio *et al., Opt. Mater. Express*, 2018, **8**, 3851 – 3863.
[111] P. Zijlstra and M. Orrit, *Rep. Prog. Phys.*, 2011, **74**, 106401.
[112] J.-H. Huh, J. Lee, and S. Lee, *ACS Photonics*, 2018, **5**, 413 – 421.
[113] I. Romero *et al.*, *Opt. Express*, 2006, **14**, 9988 – 9999.
[114] S. Marhaba *et al.*, *J. Phys. Chem. C*, 2009, **113**, 4349 – 4356.
[115] A. E. Schlather *et al.*, *Nano Lett.*, 2013, **13**, 3281 – 3286.
[116] G. Zengin *et al*., *Sci. Rep.,* 2013, **3**, 3074.
[117] G. Zengin *et al.*, *Phys. Rev. Lett.* 2015, **114**, 157401.
[118] M. Wersäll *et al.*, *Nano Lett.*, 2017, **17**, 551 – 558.
[119] A.-M. Roller *et al.*, *Nano Lett.,* 2016, **16**, 5962 – 5966.
[120] R. Liu *et al.*, *Phys. Rev. Lett.*, 2017, **118**, 237401.
[121] T. Itoh *et al*., *Phys. Rev. B*, 2014, **89**, 195436.
[122] X. Chen *et al.*, *Nano Lett.*, 2017, **17**, 3246 – 3251.
[123] J. Huang *et al*., *ACS Photonics*, 2019, **6**, 838 – 843.
[124] O. S. Ojambati *et al*., *Nat. Comms.*, 2019, **10**, 1049.
[125] J. Wen *et al.*, *Nano Lett.*, 2017, **17**, 4689 – 4697.
[126] B. Li *et al.*, *ACS Nano*, 2017, **11**, 9720 – 9727.
[127] M. Wang *et al*., *Adv. Mater.,* 2018, **30**, 1750779.
[128] M. Stührenberg *et al*., *Nano Lett.*, 2018, **18**, 5938 – 5945.
[129] J. Sun *et al*., *ACS Nano*, 2018, **12**, 10393 – 10402.
[130] T. Hartsfield *et al.*, *Proc. Natl. Acad. Sci. USA*, 2015, **112**, 12288 – 12292.
[131] R. Chikkaraddy *et al.*, *Nature*, 2016, **535**, 127 – 130.
[132] K. Santhosh *et al*., *Nat. Comms.*, 2016, **7**, 11823.
[133] Y. Zhang *et al*., *Nat. Comms.,* 2017, **8**, 15225.
[134] H. Groß *et al.*, *Sci. Adv.,* 2018, **4**, eaar4906.
[135] C. Van Vlack, P. T. Kristensen, and S. Hughes, *Phys. Rev. B*, 2012, **85**, 075303.
[136] M. L. Anderson *et al*., *Nat. Phys.*, 2011, **7**, 215 – 218.
[137] T. Neuman *et al*., *Nano Lett.*, 2018, **18**, 2358 – 2364.
[138] A. Cuartero-González and A. I. Fernández-Domínguez, *ACS Photonics*, 2018, **5**, 3416 – 3420.
[139] Y. A. Yokovlev, V. G. Nazin, and G. N. Zhizhin, *Opt. Commun.*, 1975, **15**, 293 – 295.
[140] H. Memmi *et al*., *Phys. Rev. Lett.*, 2017, **118**, 126802.
[141] E. A. Muller *et al*., *ACS Photonics*, 2018, **5**, 3594 – 3600.

FEATURE ARTICLE

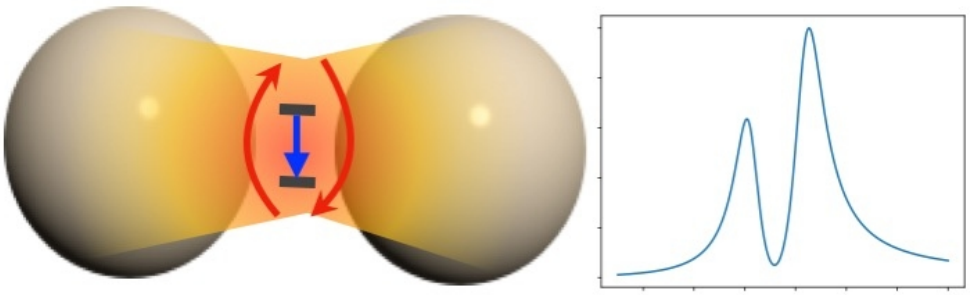

79x40mm (229 x 229 DPI)